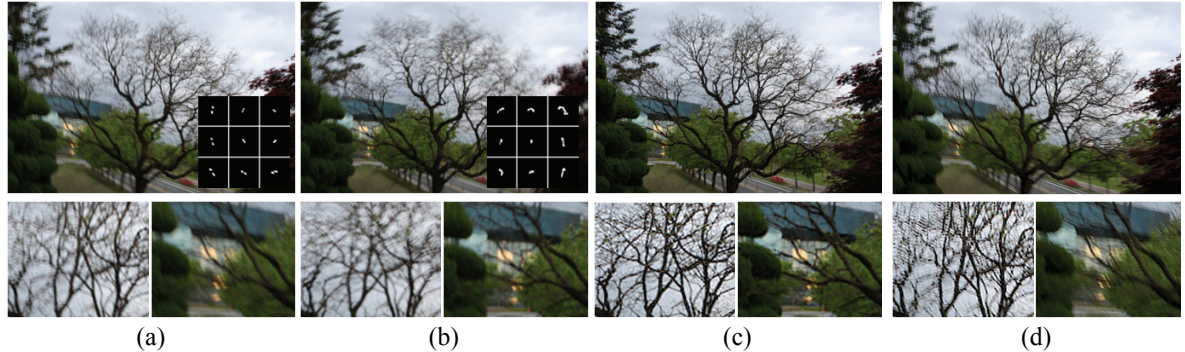


# Registration Based Non-uniform Motion Deblurring

Sunghyun Cho<sup>1</sup>      Hojin Cho<sup>1</sup>      Yu-Wing Tai<sup>2</sup>      Seungyong Lee<sup>1</sup>

<sup>1</sup>POSTECH      <sup>2</sup>KAIST



**Figure 1:** Non-uniform motion deblurring: (a)&(b) Input images and non-uniform blur kernels estimated by our method, (c) Our non-uniform motion deblurring result, (d) Uniform motion deblurring result [CL09].

## Abstract

This paper proposes an algorithm which uses image registration to estimate a non-uniform motion blur point spread function (PSF) caused by camera shake. Our study is based on a motion blur model which models blur effects of camera shakes using a set of planar perspective projections (i.e., homographies). This representation can fully describe motions of camera shakes in 3D which cause non-uniform motion blurs. We transform the non-uniform PSF estimation problem into a set of image registration problems which estimate homographies of the motion blur model one-by-one through the Lucas-Kanade algorithm. We demonstrate the performance of our algorithm using both synthetic and real world examples. We also discuss the effectiveness and limitations of our algorithm for non-uniform deblurring.

Categories and Subject Descriptors (according to ACM CCS): I.4.3 [Image Processing and Computer Vision]: Enhancement—Sharpening and deblurring

## 1. Introduction

Motion blur arises from camera shake is a common artifact when we take an image with a long exposure time. The aim of motion deblurring is to reverse the motion blur process to recover a sharp and clear image of the scene from the captured blurry image. Motion deblurring, however, is a severely ill-posed problem as the number of unknowns exceeds the number of equations that can be derived from the observed data.

A common assumption in existing motion deblurring al-

gorithms is that a motion PSF is spatially invariant, where all pixels are uniformly convolved with the same motion blur kernel. However, as recently discussed in [LWDF09], camera shake motions typically exhibit notable amounts of rotations that cause non-uniform (or spatially varying) motion blurs in captured images. For such images, motion deblurring algorithms with a uniform motion PSF may generate results with ringing artifacts due to inaccurate modeling of the true motion PSF. Image priors have been introduced to suppress ringing artifacts by regularizing amplified image

noise in deblurred images. Nevertheless, when the effect of non-uniform motion blur is large, such regularization based methods often produce less satisfactory results.

Recently a projective motion blur model [TTB11], which can fully describe the motions of camera shake in 3D world using a small number of homographies, has been proposed. The blur model can handle large motion blur consisting of translations and rotations, and even zooming blur, which is often observed in a video sequence. However, Tai et al. [TTB11] proposed only a non-blind deblurring algorithm for the blur model and assumed the motion PSF is given. Some recent techniques have tried to estimate the motion PSF of the model using coded exposure [TKLS10], video sequence [LKJ<sup>\*</sup>10], and motion sensor [JKZS10], but they need either special hardware or additional assumption on motion blur due to the difficulty of estimating a set of homographies.

As the projective motion blur model has clear benefits of covering a wide range of non-uniform blurs, natural questions would be: *Is it possible to accurately estimate non-uniform motion blur from a blurred image or images based on the model? If possible, how?* In this paper, we answer these questions by introducing a registration based non-uniform motion PSF estimation algorithm. Our idea is to adapt the matured image registration technique for solving the PSF estimation problem because homographies used in the projective blur model can represent transformations between registered images. We design a PSF estimation algorithm that solves a set of registration problems to determine the homographies. To show the effectiveness of our algorithm, we apply it to a blind deblurring framework, which uses multiple blurred images as input. Fig. 1 shows an example of our inputs and the corresponding results.

In summary, our contributions are as follows.

- We present a fully automatic non-uniform deblurring algorithm which utilizes the non-uniform motion blur model proposed in [TTB11]. We transform the non-uniform PSF estimation problem into the image registration problem, for which mature solutions have been developed. We also discuss issues and limitations of our approach.
- While there exist algorithms for non-uniform motion deblurring, those algorithms either require special hardware [TKLS10, LKJ<sup>\*</sup>10, JKZS10] or limit the degrees of freedom of camera motion in 3D world [WSZP10, GJZ<sup>\*</sup>10, HSNS11]. In contrast, our approach does not need hardware, and allows the full motion parameters of camera shake in 3D to be estimated.
- We bridge the gap between motion estimation and motion deblurring. While a PSF in motion deblurring represents motion of a camera, current deblurring algorithms can only be used to estimate a PSF, but not for camera motion. Our approach exploits the tight relationship among camera motion estimation and PSF estimation.

## 2. Related Work

Image deblurring is a longstanding problem in computer vision and image processing. Yet this problem has received a lot of attention in recent years given its utility in photography. Traditional non-blind deblurring algorithms include the well-known Richardson-Lucy algorithm [Ric72, Luc74] and Wiener filter [Wie64].

Most existing work handling image blurs due to camera motions has assumed a globally uniform PSF for an entire image. Due to poor kernel estimation or unrecoverable frequency loss from convolution, motion deblurring can introduce undesirable artifacts in the results, such as ringing and amplification of image noise. The state-of-the-art approaches deal with these artifacts by including different image priors to regularize the PSF estimation and latent image restoration processes. Representative techniques include [FSH<sup>\*</sup>06, LFDF07, YSQS07, CYTQ08, YSQS08, SJA08, CL09]. We refer readers to [LWDF09] for a review of blind motion deblurring algorithms.

These previous approaches under the uniform PSF assumption cannot handle non-translational camera motions. Recent work [LWDF09] has recognized the need for using a better motion blur model or regularization to handle spatially varying motion blurs. Shan et al. [SXJ07] handled a spatially varying blur by restricting the relative motion between the camera and the scene to be a global in-plane rotation. Tai et al. [TDBL08] used a hybrid camera [BEN03] to estimate per-pixel PSFs using an auxiliary video camera. Dai and Wu [DW08] used an alpha matte to estimate a spatially varying motion PSF. However, these approaches rely on the conventional kernel based PSF model for spatially varying motion blurs. Not only does the model require significant storage to represent per-pixel PSFs, but it also significantly complicates the deblurring process by forcing each pixel to be handled independently.

After Tai et al. [TTB11] introduced the projective motion blur model, several follow-up approaches have been proposed. (An early version of [TTB11] was available online as a technical report since 2009, and some of the follow-up approaches cited the technical report.) Whyte et al. [WSZP10] proposed a non-uniform blur model, which assumes the motion blur model contains only rotational motions of a camera. Gupta et al. [GJZ<sup>\*</sup>10] estimated non-uniform blur that consists of in-plane translations and rotations. Hirsch et al. [HSNS11] combines a patch-wise uniform motion blur model [HSSH10] and the rotational model in [WSZP10] to estimate a non-uniform PSF efficiently. These methods have limitations in that they can handle only three degrees of freedom for camera motion in 3D world. Joshi et al. [JKZS10] proposed a method that can fully estimate all of the six degrees of freedom of camera motion in 3D, but it uses hardware motion inertia sensors. Cho et al. [CW12] used homographies with eight degrees of freedom to approximate non-uniform motion blur in video frames, but their approach

needs tracking data between video frames. In this paper, we explore a deblurring solution that takes the full advantage of the projective motion blur model for six degrees of freedom of camera motion, without using any special hardware.

### 3. Non-uniform Motion Blur Model

A conventional motion blur model represents a blurred image  $B$  as a convolution of the latent image  $L$  with a spatially invariant motion PSF  $K$  plus additional image noise  $N$ :

$$B(\mathbf{x}) = K \otimes L(\mathbf{x}) + N(\mathbf{x}), \quad (1)$$

where  $\otimes$  is the convolution operator and  $\mathbf{x}$  is a vector representation of a pixel position. In the image formation process, a pixel intensity of an image is determined by the amount of light (photons) received during the exposure period. Assuming there is no moving object and the scene captured has no depth variations, the conventional motion blur model can be expressed as:

$$\mathbf{b} = \sum_i w_i \mathbf{T}_i \mathbf{l} + \mathbf{n}. \quad (2)$$

$\mathbf{b}$ ,  $\mathbf{l}$ , and  $\mathbf{n}$  are the  $n \times 1$  vector representations of  $B$ ,  $L$ , and  $N$ , respectively, where  $n$  is the number of pixels in image  $B$ .  $\mathbf{T}_i$  is an  $n \times n$  transformation matrix that produces a 2D translation of the image  $\mathbf{l}$ . It represents the in-plane translational motion of a camera at time  $t_i$  during the exposure period, which can be parametrized by a 2D vector.  $w_i$  is a weight representing the proportion, i.e.,  $\sum_i w_i = 1$ , of time spent by the camera in that pose.

When a camera shake contains only translational motions, Eqs. (1) and (2) are simply different representations of the same model. However, if a camera shake includes non-translational motions, Eq. (1) cannot be immediately extended to represent non-uniform spatially varying motion blurs in  $B$ . In contrast, in Eq. (2), we can easily replace  $\mathbf{T}_i$  by a general homography  $\mathbf{P}_i$ , and obtain a new non-uniform motion blur model for a camera shake [TTB11]:

$$\mathbf{b} = \sum_i w_i \mathbf{P}_i \mathbf{l} + \mathbf{n}. \quad (3)$$

Comparing Eq. (3) with Eq. (2), we have a significantly larger number of variables to estimate. A translation  $\mathbf{T}_i$  has two independent parameters but a homography  $\mathbf{P}_i$  contains eight parameters. While the conventional blind motion deblurring problem has already been known to be ill-posed, a blind motion deblurring algorithm for this new blur model is even more challenging. Fortunately, as we will present in the next section, we can *transfer this ill-posed problem into a well-posed image registration problem* that allows us to solve the blind motion deblurring problem effectively. This intuitive formulation and the solution process are the major contributions of this paper.

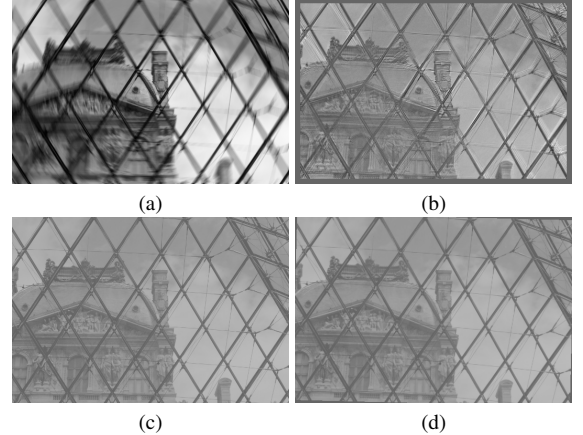


**Figure 2:** Image registration for kernel update. (a) Input motion blurred image, (b) Residual image  $e_i$ , (c) Attenuated latent image  $w_i l$ , (d) Registered image  $w_i P_i l$ . Image brightness in (b), (c), and (d) were enhanced for visualization.

### 4. PSF Estimation

In this section, we describe our non-uniform PSF estimation method, which estimates a non-uniform PSF from a given blurred image and a latent sharp image. Such estimation is an important component of many blind deblurring systems, which alternately update a latent image and a PSF [SJA08, CL09, HSHS11]. In the next section, we will apply the PSF estimation method into a blind deblurring process, which uses multiple blurred images.

Given a blurred image  $\mathbf{b}$  and a latent image  $\mathbf{l}$ , we want to estimate PSF parameters  $(\mathbf{P}, \mathbf{w})$  using the blur model in Eq. (3), where  $\mathbf{P}$  and  $\mathbf{w}$  are the sets of homographies  $\{\mathbf{P}_i\}$  and weights  $\{w_i\}$ , respectively. We define the objective function for PSF estimation as:

$$\arg \min_{\mathbf{P}, \mathbf{w}} \|\mathbf{b} - \sum_i w_i \mathbf{P}_i \mathbf{l}\|^2 + \lambda_{\mathbf{P}} \mathcal{P}_{\mathbf{P}}(\mathbf{P}) + \lambda_{\mathbf{w}} \mathcal{P}_{\mathbf{w}}(\mathbf{w}), \quad (4)$$

where  $\lambda_{\mathbf{P}} \mathcal{P}_{\mathbf{P}}(\cdot)$  and  $\lambda_{\mathbf{w}} \mathcal{P}_{\mathbf{w}}(\cdot)$  are the relative weights and priors for regularization of  $\mathbf{P}$  and  $\mathbf{w}$ , respectively.

Without loss of generality, we can rearrange the order of homographies in Eq. (3) and obtain

$$\mathbf{b} - \sum_{j \neq i} w_j \mathbf{P}_j \mathbf{l} = w_i \mathbf{P}_i \mathbf{l} + \mathbf{n}, \quad (5)$$

where the left-hand side is the residual image  $\mathbf{e}_i$  for the homography  $\mathbf{P}_i$ . Assuming the image noise  $\mathbf{n}$  is small, we can transform the PSF estimation problem into an image registration problem by finding  $\mathbf{P}_i$  that minimizes the difference between  $w_i \mathbf{P}_i \mathbf{l}$  and  $\mathbf{e}_i$  (Fig. 2). That is, we solve

$$\arg \min_{\mathbf{P}_i} \|\mathbf{e}_i - w_i \mathbf{P}_i \mathbf{l}\|^2 + \lambda_{\mathbf{P}} \mathcal{P}_{\mathbf{P}}(\mathbf{P}_i), \quad (6)$$

where the residual image is  $\mathbf{e}_i = \mathbf{b} - \sum_{j \neq i} w_j \mathbf{P}_j \mathbf{l}$ .

**Algorithm 1: PSF Estimation**


---

Input:  $\mathbf{I}^t, \mathbf{P}^{t-1}, \mathbf{w}^{t-1}$   
Output:  $\mathbf{P}^t, \mathbf{w}^t$   
Iterate for  $iter = 1 : N\_iters$   
    Iterate for  $i = 1 : p$  (# of homographies)  
        estimate  $\mathbf{P}_i$  using Eq. (6)  
    end for  
    estimate  $\mathbf{w}$  using Eq. (9)  
end for

---

This minimization can be handled using a Lucas-Kanade based image registration method [BM04]. Hence, for fixed  $\mathbf{I}$  and  $\mathbf{w}$ , we can estimate  $\mathbf{P}$  by obtaining  $\mathbf{P}_i$  one by one using Eq. (6). To regularize the image registration process, we set the prior  $\mathcal{P}_{\mathbf{P}}(\mathbf{P}_i) = \|\mathbf{P}_i - \mathbf{P}_i^o\|^2$ , where  $\mathbf{P}_i^o$  is the current homography before update, obtained in the previous iteration (see Algorithm 1). In our implementation, we use  $\lambda_{\mathbf{P}} = 1$ .

To obtain  $\mathbf{w}$ , we rewrite Eq. (3) as

$$\mathbf{b} = \mathbf{L}\mathbf{w} + \mathbf{n}, \quad (7)$$

where  $\mathbf{L} = [\mathbf{P}_1\mathbf{I} \ \mathbf{P}_2\mathbf{I} \ \dots \ \mathbf{P}_p\mathbf{I}]$  is an  $n \times p$  matrix and  $p$  is the number of homographies. We solve Eq. (7) by

$$\arg \min_{\mathbf{w}} \|\mathbf{b} - \mathbf{L}\mathbf{w}\|^2 + \lambda_{\mathbf{w}} \mathcal{P}_{\mathbf{w}}(\mathbf{w}), \quad (8)$$

where we set the prior  $\mathcal{P}_{\mathbf{w}}(\mathbf{w}) = \|\mathbf{w}\|^2$  to avoid singularity of matrix inverse. Since  $n \gg p$ , Eq. (8) can be solved effectively using a non-negative least square method, subject to  $\sum_i w_i = 1$ , by computing

$$\mathbf{w} = (\mathbf{L}^T \mathbf{L} + \lambda_{\mathbf{w}} \mathbf{I})^{-1} \mathbf{L}^T \mathbf{b}. \quad (9)$$

In our implementation, we set  $\lambda_{\mathbf{w}} = 0.1$ .

Algorithm 1 summarizes the PSF update process. We use  $N\_iters = 10$  for updating  $(\mathbf{P}, \mathbf{w})$  in the PSF estimation step before switching to the latent image restoration step.

**PSF estimation with camera intrinsic parameters** If the information about the camera is available, we can further restrict the parameters of homographies  $\mathbf{P}$ . Let  $\widehat{\mathbf{P}}_i$  be the  $3 \times 3$  homography matrix corresponding to the  $n \times n$  matrix representation  $\mathbf{P}_i$ , where  $n$  is the number of pixels. We can rewrite each  $\widehat{\mathbf{P}}_i$  as

$$\widehat{\mathbf{P}}_i = \mathbf{K}(\mathbf{R}_i + \mathbf{T}_i)\mathbf{K}^{-1}, \quad (10)$$

where  $\mathbf{K}$  is the camera intrinsic matrix, which can be obtained from the EXIF tags of photographs,  $\mathbf{R}_i$  is a  $3 \times 3$  rotational matrix, and  $\mathbf{T}_i$  is a  $3 \times 3$  translational matrix. As a result, six parameters (three for  $\mathbf{R}_i$  and three for  $\mathbf{T}_i$ ) are sufficient to describe each homography  $\widehat{\mathbf{P}}_i$ . Based on this decomposition, we can estimate a homography in a more efficient and reliable way using the Lucas-Kanade algorithm as described in [SS97]. Moreover, we can further reduce the

number of parameters in a homography by making an assumption about the camera motion (e.g., no z-axis translation or no out-of-plane rotation). For detailed derivation of the Lucas-Kanade algorithm using camera intrinsic parameters, we refer a reader to [SS97].

## 5. Deblurring with Multiple Blurred Images

In this section, we describe a blind motion deblurring algorithm which uses the PSF estimation method described in Sec. 4. For blind motion deblurring, we take multiple blurred images as input because using multiple images is known to be more robust and produce higher quality results than single image deblurring [YSQS07, CYTQ08]. As pointed out by [LWDF09], single image deblurring needs something more than simple maximum a posteriori (MAP) estimation based alternating optimization because sparsity priors prefer blurry images to sharp ones and such alternating optimization can result in the trivial solution of a delta function PSF. To overcome this problem, for example, Cho and Lee [CL09] used a prediction scheme and Fergus et al. [FSH\*06] used a variational Bayesian approach. We will discuss about single image deblurring based on our PSF estimation in Sec. 7.

When we use multiple blurred images as input, the images contain information of the same scene even though their amount and distribution of blurs may differ. The major advantage of this setting is that we can benefit from the mutually complementary information of the scene in the input images. Such information helps to avoid the trivial solution problem of single image deblurring. It effectively suppresses ringing artifacts and image noise, as well as artifacts caused by saturated regions during latent image restoration. We can also achieve higher accuracy of PSF estimation with better estimation of the latent image.

Mathematically, we want to solve the following optimization problem:

$$\begin{aligned} \arg \min_{\mathbf{I}, \mathbf{P}, \mathbf{w}} & \sum_k \left\| \mathbf{b}_k - \sum_i w_{(k,i)} \mathbf{P}_{(k,i)} \mathbf{I} \right\|^2 \\ & + \lambda_{\mathbf{I}} \mathcal{P}_{\mathbf{I}}(\mathbf{I}) + \lambda_{\mathbf{P}} \mathcal{P}_{\mathbf{P}}(\mathbf{P}) + \lambda_{\mathbf{w}} \mathcal{P}_{\mathbf{w}}(\mathbf{w}), \end{aligned} \quad (11)$$

where  $k$  is the index for input images, and  $\lambda_{\mathbf{I}} \mathcal{P}_{\mathbf{I}}(\cdot)$  is the relative weight and regularization prior of  $\mathbf{I}$ .

A common approach to this type of optimization is to divide the problem into two closely related subproblems, and to solve each subproblem alternately and iteratively. In this paper, we follow this direction and divide the problem into PSF  $(\mathbf{P}, \mathbf{w})$  estimation and latent image  $\mathbf{I}$  restoration.

**PSF estimation with multiple blurred images** We use the method described in Sec. 4 to obtain the motion PSF individually for each input image. Suppose we have two motion blurred input images,  $\mathbf{b}_1$  and  $\mathbf{b}_2$ . In the first iteration, we use the second image  $\mathbf{b}_2$  as the latent image  $\mathbf{I}^1$  to estimate

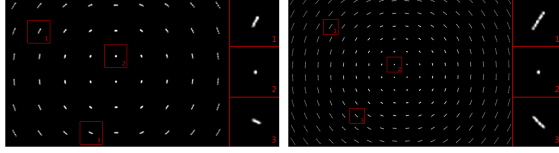


**Figure 3:** Estimated motion PSFs at different scales. For visualization purpose, we construct the PSFs by applying the homographies to the impulse values at regularly sampled pixel locations. Note that the density and the shape of a PSF become refined from a coarse to the finer scales.

the initial PSF  $(\mathbf{P}_{(1,i)}^1, \mathbf{w}_{(1,i)}^1)$  of the first image  $\mathbf{b}_1$ . The single image deblurring result of  $\mathbf{b}_1$  is then used to estimate the initial PSF  $(\mathbf{P}_{(2,i)}^1, \mathbf{w}_{(2,i)}^1)$  of the second image  $\mathbf{b}_2$ . After we obtain the PSFs of both  $\mathbf{b}_1$  and  $\mathbf{b}_2$ , we estimate the latent image  $\mathbf{l}^2$  with the latent image restoration method using Eq. (12). Then, the algorithm continues using  $\mathbf{l}^2$  as the latent image for estimating the PSF of each image in the next iteration.

**Latent image restoration with multiple blurred images** To obtain the latent image  $\mathbf{l}$  with fixed  $(\mathbf{P}^t, \mathbf{w}^t)$ , we need to solve

$$\arg \min_{\mathbf{l}} \sum_k \|\mathbf{b}_k - \sum_i w_{(k,i)}^t \mathbf{P}_{(k,i)}^t \mathbf{l}\|^2 + \lambda_{\mathbf{l}} \mathcal{P}_{\mathbf{l}}(\mathbf{l}). \quad (12)$$

This is a non-blind motion deblurring problem, which can be solved effectively using the approach in [TTB11]. In our implementation, we set  $\lambda_{\mathbf{l}}$  as 0.005 and  $\mathcal{P}_{\mathbf{l}}(\mathbf{l})$  as

$$\mathcal{P}_{\mathbf{l}}(\mathbf{l}) = (\|\mathbf{D}_x \mathbf{l}\|_{\alpha})^{\alpha} + (\|\mathbf{D}_y \mathbf{l}\|_{\alpha})^{\alpha}, \quad (13)$$

where  $\mathbf{D}_x$  and  $\mathbf{D}_y$  are the  $x$ - and  $y$ -direction partial differential operators in the matrix form, respectively.  $\|\cdot\|_{\alpha}$  is the  $L_{\alpha}$  norm of a vector, while  $\|\cdot\|$  denotes the  $L_2$  norm in this paper. We set  $\alpha = 0.8$ , which gives a sparsity prior [LFDF07] to suppress ringing artifacts and image noise in latent image restoration. To solve Eq. (12), we implemented the iterative reweighted least square method [LFDF07].

**Multi-scale implementation** To avoid poor local minima, and to increase the stability of the algorithm, we adopt a multi-scale approach using a Gaussian pyramid. The upsampling factor  $s$  from one level to the next is two. We estimate the motion PSF and the latent image from coarse to fine levels, where the PSF and latent image estimated at a coarse level are upsampled and used as initial values for iterative optimization in the next finer level. At the coarsest level, we use  $\mathbf{P}_i = \mathbf{I}$  and  $w_i = 1/p$  for initial homographies and weights  $(\mathbf{P}^0, \mathbf{w}^0)$ . For the initial latent image  $\mathbf{l}^1$  at the coarsest level, we use the downsampled version of another image among multiple input images, as described before.

At the coarsest level, we use only a few number (e.g., four) of homographies to approximate the motion PSF. When we move from a coarse to the finer level, we quadruple the num-

ber of homographies used for representing the motion PSF. Since the width and height of an image are doubled, we need to quadruple the sampling rate of homographies to catch up the increased sampling rate of image details. Increasing the sampling rate of homographies also allows us to achieve finer refinement of the estimated motion PSF (Fig. 3).

Let  $\{\dots, (\widehat{\mathbf{P}}_i, w_i), \dots\}$  be the set of estimated motion PSFs at a coarse level. The corresponding initial value of  $(\widehat{\mathbf{P}}, \mathbf{w})$  at the next finer level is  $\{\dots, (\widehat{\mathbf{P}}_i^1, \frac{w_i}{4}), (\widehat{\mathbf{P}}_i^2, \frac{w_i}{4}), (\widehat{\mathbf{P}}_i^3, \frac{w_i}{4}), (\widehat{\mathbf{P}}_i^4, \frac{w_i}{4}), \dots\}$ , where

$$\widehat{\mathbf{P}}_i^j = \begin{bmatrix} s & 0 & t_x^j \\ 0 & s & t_y^j \\ 0 & 0 & 1 \end{bmatrix} \widehat{\mathbf{P}}_i \begin{bmatrix} \frac{1}{s} & 0 & 0 \\ 0 & \frac{1}{s} & 0 \\ 0 & 0 & 1 \end{bmatrix}. \quad (14)$$

$(t_x^j, t_y^j) \in \{(0,0), (\frac{1}{2}s, 0), (0, \frac{1}{2}s), (\frac{1}{2}s, \frac{1}{2}s)\}$  is the translation for the increased sampling rate. Before upsampling, we drop the homographies with weights less than  $0.01 \times \max\{w_i\}$  to maintain a small number of homographies.

## 6. Results

For experiments, we implemented our method using C++. We used a PC with an Intel Core i7 3GHz and 12GB RAM. Fig. 4 shows examples of our method. All input images were blurred by real camera shakes. Every input image is  $600 \times 400$ . We typically used three to four levels for the multi-scale blur estimation, and estimated about 32 homographies for each blurred input image. For every test case, it took about 100 seconds to generate a deblurring result, where most computation was used for image registration. More deblurring results can be found in the supplementary material.

We use a synthetic example to compare the deblurring result of our method with previous methods [WSZP10, CL09, SJA08, FSH\*06] (Fig. 5). For comparison with [WSZP10], we did not implement their variational Bayesian approach. Instead, we constrain the parameters of our homography model to contain only rotational motions. Hence, the results of [WSZP10] shown in this paper are *our results from multiple input images* but with their model, which is more restrictive than our model. The methods of Cho and Lee [CL09], Shan et al. [SJA08], and Fergus et al. [FSH\*06] are for single image blind motion deblurring. While our approach uses multiple input images, we run their methods on each input image, and pick the best result. We know that this comparison is not entirely fair, but still expect it can give some useful information.

In Fig. 5, the motion blurs of the two input images contain rotational (both in-plane and out-of-plane) and translational motions. We show the deblurring results with magnified views and difference images from the ground truth image. Table 1 compares the restoration errors quantitatively using PSNR. Our approach produces visually and quantitatively the least amount of errors compared to previous meth-

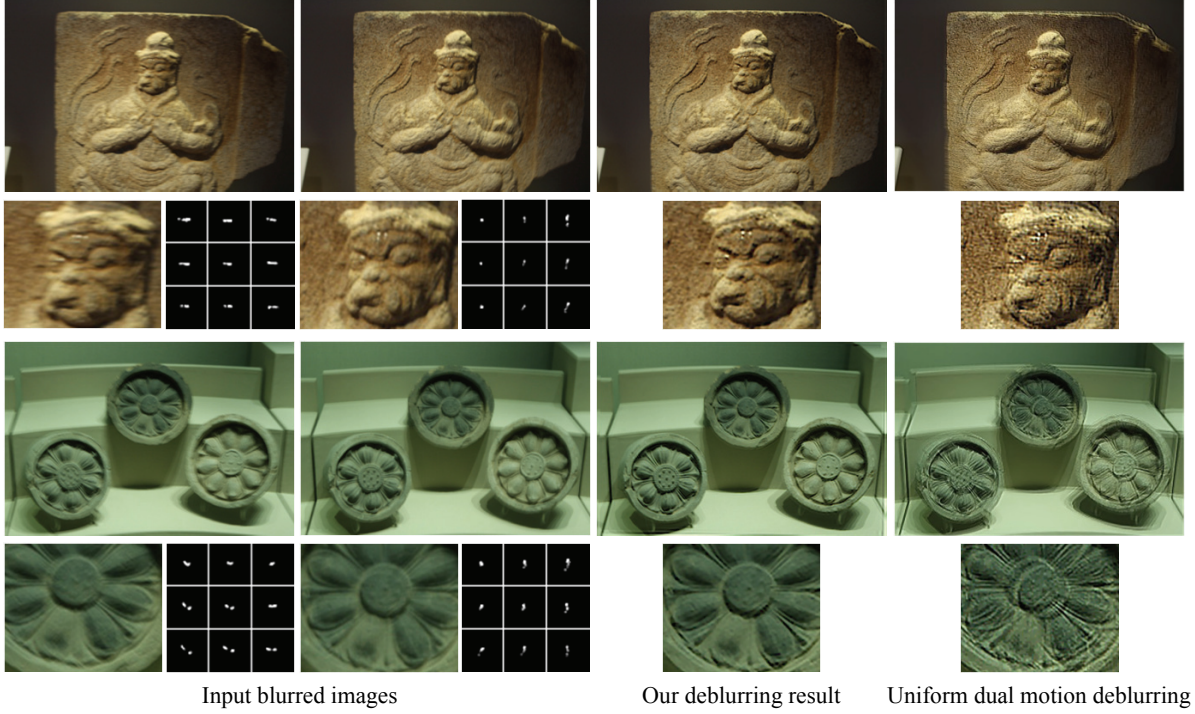


**Figure 4:** Deblurring examples with real images. For uniform dual motion deblurring, we extended a single image deblurring method [CL09] to restore the latent image from multiple input images. The PSFs estimated by our method for different image regions are shown with the input images.

Method	PSNR
Our method	32.5257
Whyte et al. [WSZP10]	31.3315
Cho and Lee [CL09]	30.5990
Shan et al. [SJA08]	30.6280
Fergus et al. [FSH*06]	30.2384

**Table 1:** Peak signal-to-noise ratio (PSNR) of the deblurring results in Fig. 5

ods. The ground truth PSFs and the estimated PSFs are also shown in Fig. 5 to demonstrate the accuracy of our PSF estimation.

In addition to our deblurring results with real examples, Fig. 4 shows the results of uniform dual motion deblurring, which is implemented by extending a single image deblurring method [CL09] to restore the latent image from multiple input images, because the implementation of a recent dual motion deblurring method [CYTQ08] is not available. From the deblurring results, we can see that uniform dual motion deblurring cannot properly handle non-uniform motions despite two input images.

Fig. 6 shows a comparison of our method with [WSZP10] using real blurred images. The results clearly show the ben-

efit of our more general non-uniform blur model over the rotation-only blur model of [WSZP10], especially for a near scene.

While most previous non-uniform deblurring methods assume that camera shakes consist of rotational and translational motions, video frames may have zooming blur as well. Fig. 7 shows an example of zooming blur. The input images are two different frames from a blurry video, and the left image of Fig. 7(a) shows significant blur due to a zooming motion. As our method can handle 8D camera motions, it successfully estimated the zooming blur and restored a sharp image (Fig. 7(b)). In contrast, three degrees of freedom for camera rotations in the blur model of [WSZP10] could not resolve the zooming blur (Fig. 7(c)).

## 7. Discussion and Future Work

In this paper, we proposed a deblurring method which can effectively handle non-uniform motion blur effects in real photographs. Our major contribution is the blind motion deblurring algorithm which transforms the PSF estimation problem into an image registration problem. While our current implementation uses multiple motion blurred images as input, we believe that this framework can be extended to single image deblurring if it is equipped with a more robust registration

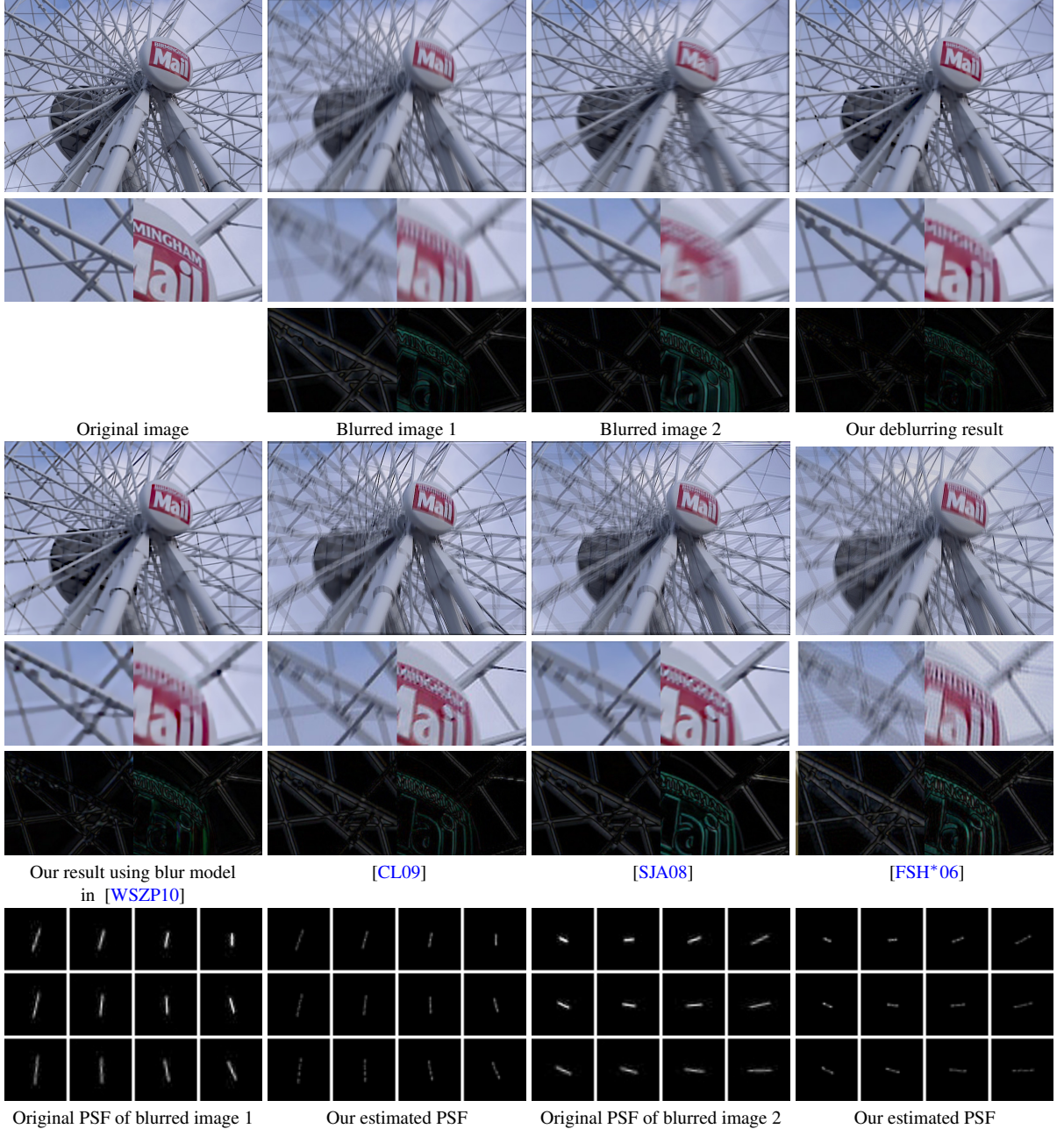


**Figure 5:** Comparison of deblurring results using a synthetic example. The first PSF on the left contains  $y$ -translation with  $x$ -axis and  $z$ -axis rotations, and the second PSF on the right contains  $x$ -translation with  $y$ -axis and  $z$ -axis rotations.

method. In the following, we discuss some issues related to our deblurring method.

**Degrees of freedom in camera motion** The motion blur model using homographies allows eight degrees of freedom. In practice, the camera motion in 3D world has only six degrees of freedom for rotations and translations. The addi-

tional two degrees of freedom correspond to the unknowns in camera intrinsic parameters. Whyte et al. [WSZP10] commented that using only three degrees of freedom for rotation is sufficient for non-uniform spatially varying motion deblurring. While this comment is correct when the focal length is long, it becomes invalid when the focal length becomes short.

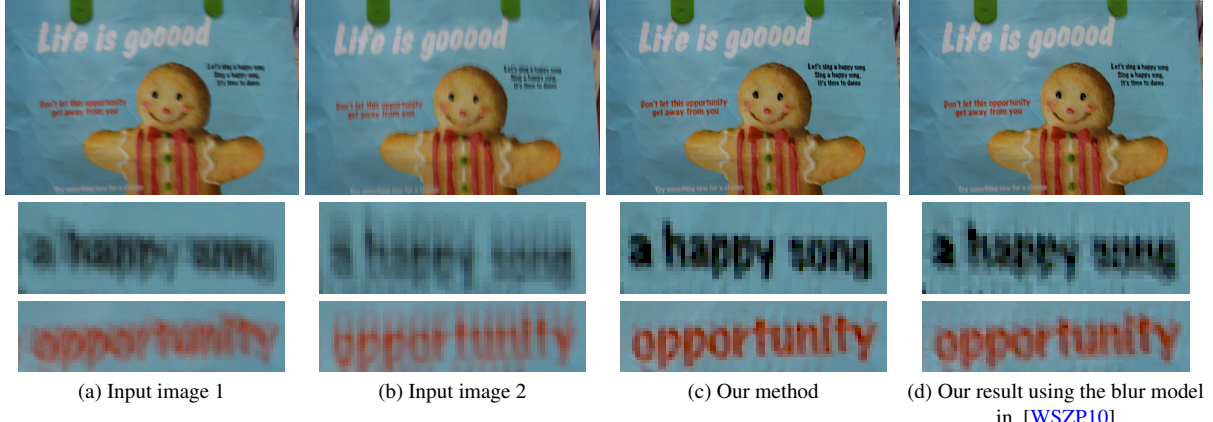


**Figure 6:** Comparison of our method with [WSZP10]. The magnified views clearly show that our general non-uniform blur model using homographies helps generate better deblurring results than the restrictive model of [WSZP10] using only rotations.

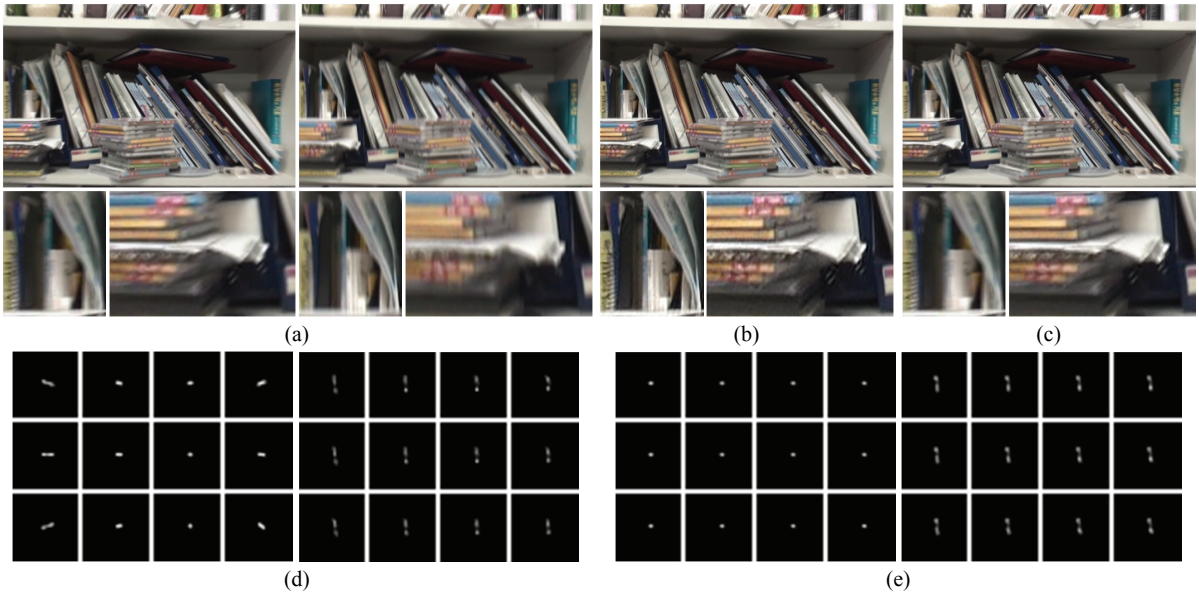


**Figure 7:** Deblurring results of real images with zooming blur. (a) Input images. (b) Deblurring result of our method. (c) Our result using the blur model in [WSZP10]. (d) & (e) Estimated PSFs for (a) to produce (b) and (c), respectively.

The rotational blurs considered in [WSZP10] assume the rotation axes to be at the image center. However, in real cases, rotational axes can be out of image center, as shown in Fig. 1. Off-center rotational motions cannot be described by homographies without translational components, especially when the focal length is small. Consequently, even for a distant scene, if the focal length is small, we cannot ignore translational components in a camera motion. Fig. 8(a) shows an example of in-plane rotational blur, whose center is at the top-left corner of the image. We approximated the in-plane rotational blur using homographies that contain only

rotational components (Fig. 8(b)), where translations were approximated by rotations with the focal length of 24mm. Figs. 8(c) and 8(d) show the approximated non-uniform blur much differs from the original, demonstrating a clear advantage of the blur model based on general homographies.

Joshi et al. [JKZS10] also measured a camera motion using motion inertia sensors and validated that the camera motion indeed has six degrees of freedom. Their deblurring algorithm requires the information from all six degrees of freedom among which translations cannot be ignored. In our ex-

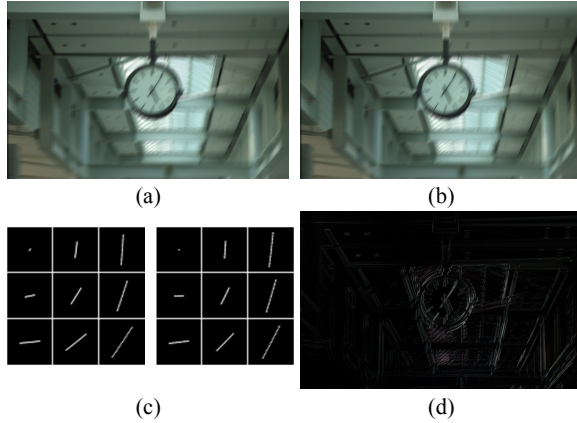


**Figure 8:** Off-center rotational blur. (a) Blurred image by an in-plane rotational motion, where the rotational center is at the top left corner of the image. (b) Image blurred by only rotational motions without translational motions, which best approximate the non-uniform blur in (a). (c) PSFs of (a) & (b). (d) Difference between (a) & (b).

periments, we compared our results with eight, six, and three degrees of freedom. The results with eight and six degrees of freedom are similar, but the results with only three degrees of freedom could degrade significantly.

**Number of homographies** For selecting the number of homographies, we adopted a simple and intuitive approach. As explained in Sec. 5, we initially use four homographies at the coarsest level, and quadruple the number when moving to the next finer level, while discarding homographies with small weights. In our experiments on  $600 \times 400$  images, about 32 homographies were typically estimated. However, since the number of homographies is closely related to the non-zero pixels in PSF, the number of homographies would increase if the blur size is large. Note that an insufficient number of homographies cannot fully express blur in an image, which leads to a blurry latent image. On the other hand, a too large number of homographies leads to slow convergence. So there is a trade-off between accuracy and running time in PSF estimation.

**Registration between blurred images** Previous methods using multiple images for deblurring (e.g., [YSQS07, CYTQ08]) require a preprocessing step to register input images. However, registration among blurry images is difficult due to ambiguities in blurry edges. In contrast, our method embeds the registration step into the PSF estimation process, and is free from this preprocessing.

**Other possible solutions** Although we proposed a novel method to estimate non-uniform motion PSFs using image registration, we note that there might be other solutions, e.g., using hardware approaches [TKLS10, LKJ<sup>\*</sup>10, JKZS10] or variational Bayesian approach [WSZP10]. The

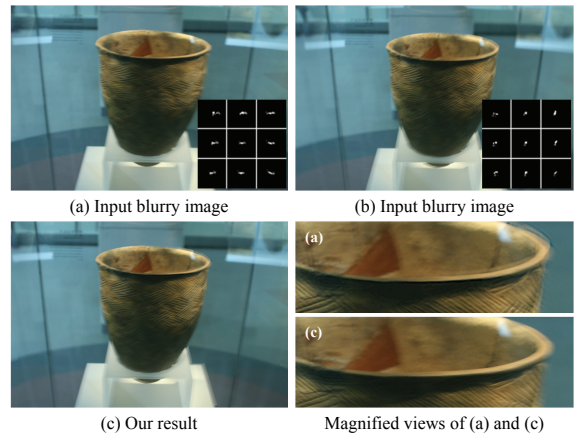


**Figure 9:** Failure example. Due to the non-linearity of the optimization process, our method could fail to estimate blurs correctly, and the result image may have remaining blur.

method in [WSZP10], however, requires quantization of the solution space and is not scalable to a large number of variables. Therefore, they reduced the number of variables by making an assumption that the camera motion contains only rotations (both in-plane and out-of-plane). In contrast, our approach does not need to make a restrictive assumption about the camera motion. Furthermore, we can handle the camera intrinsics as unknowns by using general homographies. Hence, our approach can be considered more general than [WSZP10].

**Single image versus multiple images** One major drawback of our method is the requirement of multiple input images. Many recent single image blind deconvolution approaches use image gradients for estimating a blur kernel [FSH<sup>\*</sup>06, CL09]. Unfortunately, we found that Lucas-Kanade image registration methods, which our blur kernel estimation method relies on, do not work well for gradient images, because most gradient values of an image are close to zero, and even an incorrect homography does not introduce large error values.

While the requirement of multiple input images may restrict the applications of our approach, using multiple input images offers several advantages. In single image deblurring, as discussed in [LWDF09], alternating optimization for a MAP solution favors the delta function solution. In multiple image deblurring, we can effectively avoid such a trivial solution because the solution does not satisfy the constraints from multiple images. Using multiple images for deblurring is also effective in suppressing artifacts, such as amplified noise and ringing, and better handles saturated regions.

**Practical issues, limitations, and future work** Our approach uses multiple motion blurred images as input. If the input images do not contain the same scene information,

e.g., different poses of a person and change of white balance due to a time gap between two captures, our algorithm would fail. However, nowadays, digital cameras usually allow a user to capture several images in a row while holding down the shutter button. Such camera setup enables avoiding the possible problems caused by a long time gap between consecutive captures. In future, we will investigate on making our algorithm robust to outliers, e.g., moving objects and exposure changes between multiple blurred images.

We found that our proposed algorithm sometimes converges to unsatisfactory results. One reason is that our algorithm estimates the homographies one-by-one individually without considering the continuity of a camera motion. Another reason is that the Lucas-Kanade method may converge to a local minimum since it is based on non-linear optimization. Fig. 9 shows a failure example.

Our method assumes that two input images have sufficiently orthogonal blurs. If input images are affected by similar blurs, e.g., blurs in the same direction, an input image cannot play the role of the latent image for the other in PSF estimation (Sec. 4), and as a result, our method may fail to converge to the right solution. A failure example of this case can be found in the supplementary material.

In future, we will study how to improve the robustness of our method. One possible direction is to extend our method to video deblurring where the motion trajectory of camera in the entire video sequence can be used to stabilize the homography estimation as well as to deblur the motion blurred frames. We will also study how to handle other types of non-uniform blurs, such as blurs from depth variations or object motions.

**Acknowledgements** We thank the anonymous reviewers for their constructive comments. We thank Flickr users kate nev (Fig. 2) and ell brown (Fig. 5) for sharing their images. This work was supported in part by Industrial Strategic Technology Development Program of KEIT (KI001820), Basic Science Research Program of NRF (2010-0019523), and NRF grant (2011-0013349).

## References

- [BEN03] BEN-EZRA M., NAYAR S.: Motion deblurring using hybrid imaging. In *Proc. CVPR* (2003). [2](#)
- [BM04] BAKER S., MATTHEWS I.: Lucas-kanade 20 years on: A unifying framework. *International Journal of Computer Vision (IJCV)* 56, 3 (2004), 221–255. [4](#)
- [CL09] CHO S., LEE S.: Fast motion deblurring. *ACM Trans. Graphics* 28, 5 (2009), article no. 145. [1, 2, 3, 4, 5, 6, 7, 9](#)
- [CWL12] CHO S., WANG J., LEE S.: Video deblurring for handheld cameras using patch-based synthesis. *ACM Trans. Graphics* 31 (2012), 64:1–64:9. [2](#)
- [CYTQ08] CHEN J., YUAN L., TANG C.-K., QUAN L.: Robust dual motion deblurring. In *Proc. CVPR* (2008). [2, 4, 6, 9](#)
- [DW08] DAI S., WU Y.: Motion from blur. In *Proc. CVPR* (2008). [2](#)
- [FSH\*06] FERGUS R., SINGH B., HERTZMANN A., ROWEIS S. T., FREEMAN W.: Removing camera shake from a single photograph. *ACM Trans. Graphics* 25, 3 (2006), 787–794. [2, 4, 5, 6, 7, 9](#)
- [GJZ\*10] GUPTA A., JOSHI N., ZITNICK L., COHEN M., CURLESS B.: Single image deblurring using motion density functions. In *Proc. ECCV* (2010). [2](#)
- [HSHS11] HIRSCH M., SCHULER C., HARMELING S., SCHOLKOPF B.: Fast removal of non-uniform camera shake. In *Proc. ICCV* (2011). [2, 3](#)
- [HSSH10] HIRSCH M., SRA S., SCHÄULKOPF B., HARMELING S.: Efficient filter flow for space-variant multiframe blind deconvolution. In *Proc. CVPR* (2010). [2](#)
- [JKZS10] JOSHI N., KANG S. B., ZITNICK L., SZELISKI R.: Image deblurring with inertial measurement sensors. *ACM Trans. Graphics* 29, 3 (2010). [2, 8, 9](#)
- [LFDF07] LEVIN A., FERGUS R., DURAND F., FREEMAN W. T.: Image and depth from a conventional camera with a coded aperture. *ACM Trans. Graphics* 26, 3 (2007), article no. 70. [2, 5](#)
- [LKJ\*10] LI Y., KANG S. B., JOSHI N., SEITZ S., HUTTENLOCHER D.: Generating sharp panoramas from motion-blurred videos. In *Proc. CVPR* (2010). [2, 9](#)
- [Luc74] LUCY L.: An iterative technique for the rectification of observed distributions. *Astronomical Journal* 79, 6 (1974), 745–754. [2](#)
- [LWDF09] LEVIN A., WEISS Y., DURAND F., FREEMAN W.: Understanding and evaluating blind deconvolution algorithms. In *Proc. CVPR* (2009). [1, 2, 4, 9](#)
- [Ric72] RICHARDSON W.: Bayesian-based iterative method of image restoration. *J. Opt. Soc. Am.* 62, 1 (1972). [2](#)
- [SJA08] SHAN Q., JIA J., AGARWALA A.: High-quality motion deblurring from a single image. *ACM Trans. Graphics* 27, 3 (2008), article no. 73. [2, 3, 5, 6, 7](#)
- [SS97] SZELISKI R., SHUM H.-Y.: Creating full view panoramic image mosaics and texture-mapped models. In *Proc. SIGGRAPH* (1997), pp. 251–258. [4](#)
- [SXJ07] SHAN Q., XIONG W., JIA J.: Rotational motion deblurring of a rigid object from a single image. In *Proc. ICCV* (2007). [2](#)
- [TDBL08] TAI Y.-W., DU H., BROWN M. S., LIN S.: Image/Video deblurring using a hybrid camera. In *Proc. CVPR* (2008). [2](#)
- [TKLS10] TAI Y.-W., KONG N., LIN S., SHIN S.-Y.: Coded exposure imaging for projective motion deblurring. In *Proc. CVPR* (2010). [2, 9](#)
- [TTB11] TAI Y.-W., TAN P., BROWN M.: Richardson-lucy deblurring for scenes under a projective motion path. *IEEE Trans. Pattern Analysis Machine Intelligence* 33, 8 (2011), 1603–1618. [2, 3, 5](#)
- [Wie64] WIENER N.: *Extrapolation, Interpolation, and Smoothing of Stationary Time Series*. MIT Press, 1964. [2](#)
- [WSZP10] WHYTE O., SIVIC J., ZISSERMAN A., PONCE J.: Non-uniform deblurring for shaken images. In *Proc. CVPR* (2010). [2, 5, 6, 7, 8, 9](#)
- [YSQS07] YUAN L., SUN J., QUAN L., SHUM H.-Y.: Image deblurring with blurred/noisy image pairs. *ACM Trans. Graphics* 26, 3 (2007), article no. 1. [2, 4, 9](#)
- [YSQS08] YUAN L., SUN J., QUAN L., SHUM H.-Y.: Progressive inter-scale and intra-scale non-blind image deconvolution. *ACM Trans. Graphics* 27, 3 (2008), article no. 74. [2](#)